Electronic Nose With Detection Method for Alcohol, Acetone, and Carbon Monoxide in Coronavirus Disease 2019 Breath Simulation Model

Tiffany C. Miller, Salvatore Domenic Morgera, *Life Fellow, IEEE*, Stephen E. Saddow, *Senior Member, IEEE*, Arash Takshi, and Matthew Palm

***Abstract*—Electronic nose technology may have the potential to substantially slow the spread of contagious diseases with rapid signal indication. As our understanding of infectious diseases such as Corona Virus Disease 2019 improves, we expect electronic nose technology to detect changes associated with pathogenesis of the disease such as biomarkers of immune response for respiratory symptoms, central nervous system injury, and/or peripheral nervous system injury in the breath and/or odor of an individual. In this paper, a design of an electronic nose was configured to detect the concentration of a COVID-19 breath simulation sample of alcohol, acetone, and carbon monoxide mixture. After preheating for 24 hours, the sample was carried into an internal bladder of the collection vessel for analysis and data was collected from three sensors to determine suitability of these sensors for the application of exhaled breath analysis. Test results show a detection range in parts-per-million within the sensor detection range of at least 10-300 ppm. The output response of an MQ-2 and an MQ-135 sensor to a diverse environment of target gasses show the MQ-2 taking a greater length of time to normalize baseline drift compared to an MQ-135 sensor due to cross interferences with other gasses. The COVID-19 breath simulation sample was established and validated based on preliminary data obtained from parallel COVID-19 breath studies based in Edinburgh and Dortmund. This detection method provides a non-invasive, rapid, and selective detection of gasses in a variety of applications in virus detection as well as agricultural and homeland security.**

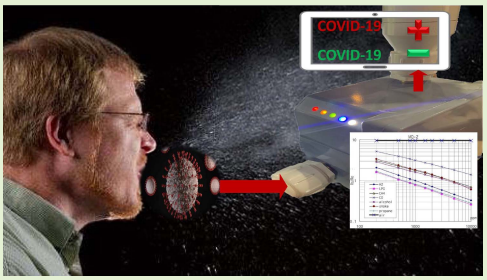

***Index Terms*— Gas sensor, alcohol and acetone detection, diagnosis model, corona virus disease-2019, electronic nose, point-of-care.**

I. Introduction

A. Observed Symptoms of COVID-19

ON MARCH 11, 2020 severe acute respiratory syndrome coronavirus 2 (SARS-CoV-2) has caused a respiratory illness pandemic in the form of Corona Virus Disease 2019 (COVID-19). A plurality of key symptoms associated with COVID-19 infections including, but not limited to: fever and dry cough accompanying approximately 80% of COVID-19 infections [4], [19] headache, nasal congestion, sore throat, nausea, labored breath or dyspnea [5]; and musculoskeletal symptoms responding to inflammatory and immune response being fatigue, myalgia or muscle pain, and arthralgia or joint pain [5], [26]. Recently observed symptoms of COVID-19 include anosmia and ageusia. Anosmia is a neurological impairment of olfactory functioning in that the olfactory system is not able to accurately detect and/or correctly identify odors and is characterized by a loss of smell. Ageusia is characterized by a loss of taste [6], [7].

Manuscript received January 24, 2021; revised April 6, 2021; accepted April 18, 2021. Date of publication April 27, 2021; date of current version July 14, 2021. This work was supported by the University of South Florida COVID-19 Rapid Response Research Award. The associate editor coordinating the review of this article and approving it for publication was Dr. Chang-Soo Kim. *(Corresponding author: Salvatore Domenic Morgera.)*

Tiffany C. Miller, Salvatore Domenic Morgera, Stephen E. Saddow, and Arash Takshi are with the Department of Electrical Engineering, University of South Florida, Tampa, FL 33620 USA (e-mail: tmillertm@usf.edu; sdmorgera@usf.edu; saddow@usf.edu; atakshi@usf.edu).

Matthew Palm is with Valhall K-9 International, LLC, Jefferson, GA 30646 USA (e-mail: matthew@valhallk9.com).

Digital Object Identifier 10.1109/JSEN.2021.3076102

B. Breath Biochemistry of COVID-19

Anosmia has been known to be an indicator of neurodegenerative diseases. Some neurological manifestations of COVID-19 result in energy failure of the neuron in response to Calcium (Ca^{+}) mediated injury to myelinated axons when an increase in the amount of sodium (Na^{+}) is retained within the inside of the cell [2]. When there is an influx of (Na^{+}) inside of a cell, the reverse operation of the (Na^{+}) - (Ca^{2+}) exchanger

is activated, thereby, importing excessive levels of (Ca^{2+}) into the axon. (Ca^{2+}) mediated injury includes, but is not limited to, fragmented neurofilaments, depolymerized microtubules, or a lowering of organelles of residual demyelinated axons [3]. An influx of (Ca^{2+}) occurs as a result from both ATP depletion and from odorant binding. For example, in odorant binding, cyclic adenosine monophosphate (cAMP) causes a depolarizing flow of current into olfactory receptor neurons, which slows odorant stimulation by closing cyclic nucleotide-gated (CNG) channels [10]. Studies have evidence supporting carbon monoxide (CO) as the diffusible intracellular and intercellular biomarker of CNG channel activity in olfactory receptor neurons. Thus, CO is a byproduct of olfactory transduction associated with CNG channel activity reduction, whereby, a loss of olfactory receptor neurons occurs for minutes [10]. These excessive concentrations of CO byproduct may be detected by a gas sensor and compared to CO concentrations of healthy individuals. In particular, studies have indicated measured concentrations of CO emitted from the breath of non-COVID-19 individuals as having approximately 2 ppm-100 ppm of CO present in their exhaled breath [13], and [14].

Although SARS-CoV-2 is considered a respiratory illness, scientific evidence demonstrates that viruses may utilize the olfactory nerve to infiltrate and damage the nervous system such as the central nervous system (CNS) and/or the peripheral nervous system (PNS) by activating T-lymphocytes which then activate microglia and inflammatory mediators [11], [12], [19], [22], [23], [24], [25]. Nervous system damage is associated with disease specific metabolites and abnormal chemical biomarkers that are emitted into the air from soft tissue samples and body cavities such as, the lungs and/or the nasal cavity, which may be detected in the breath of an individual with an electronic nose (eNose) sensor as a diagnostic test for COVID-19 [1], [8], [20], [21]. Referring to Table I, in addition to carbon monoxide being an inflammatory biomarker, preliminary data obtained from parallel COVID-19 breath studies, based in Edinburgh and Dortmund, have indicated statistically significant concentrations of methanol gas which is an alcohol and a ketone gas being acetone, using gas chromatography-ion mobility spectrometry (GC-IMS), as being capable of discriminating between patients with COVID-19 and healthy individuals [17]. For example, at the Royal Infirmary of Edinburgh (RIE), a participant's COVID-19 positive breath sample was collected within the GC-column to separate the plurality of compounds of the breath. Next, the plurality of compounds was ionized, whereby, the ions exhibited a characteristic drift time determined by the detector based on properties such as mass and charge [17]. Table I shows detected exhaled methanol monomer and methanol dimer concentrations having a relative drift time of 0.99 ms and 1.036 ms, respectively, whereby, signal processing of GC-IMS data with MATLAB and statistical analysis indicated a lower methanol signal volume emitted from exhaled breath of RIE COVID-19 positive participants compared to non-COVID-19 exhaled breath samples [17]. Although this aforementioned RIE study resulted in an identification of a decreased concentration of methanol in the exhaled breath of COVID-19 positive participants using GC-IMS and did not use a gas sensor capable of detecting methanol concentrations in ppm, the results contribute to our understanding of the COVID-19 exhaled breath pattern signature.

TABLE I
VOC CONCENTRATION TRENDS IN EXHALED BREATH OF HEALTHY SAMPLES COMPARED TO VIRAL INFILTRATED SAMPLES

VOC Type	Sensor Type	VOC Measured Values emitted from Non-COVID-19 Breath	Relative Drift Time in GC-IMS of RIE Samples of COVID-19 Breath	References
Acetone	MQ-135	0.24 ppm-1.69 ppm	1.159 ms	[15], [16], [17]
Methanol Monomer-Alcohol	MQ-2	0.4 ppm-2.0 ppm	0.99 ms	[15], [17]
Methanol Dimer-Alcohol	MQ-2	0.4 ppm – 2.0 ppm	1.036 ms	[15], [17]

Table I further shows detected exhaled acetone concentrations having a relative drift time of 1.159 ms, whereby, signal processing of this GC-IMS data with MATLAB, preliminary modeling, and statistical analysis indicated an increased acetone signal volume emitted from exhaled breath of RIE COVID-19 positive participants compared to non-COVID-19 exhaled breath samples, corresponding to an increased concentration of acetone in COVID-19 positive participants [17]. It is currently known that environmental contaminants exist in both the ambient air and/or an exhaled breath sample. For example, Table I shows concentrations of acetone in non-COVID-19 exhaled breath samples having a detected concentration range between 0.24 ppm-1.69 ppm [17]. Hence, a gas sensor, such as the MQ-135, capable of detecting acetone at levels exceeding 1.69 ppm is desirable for the application of detection of breath acetone levels. In addition, the reduction of environmental contaminants within ambient air can be reduced and/or eliminated with an air tight sample collection and processing system. Thus, the simulated breath sample solution of this current simulation model was based from the aforementioned breath studies and comprises CO, alcohol and acetone within an air tight sample collection and processing system.

II. METHOD AND EXPERIMENT

A. Electronic Nose

The electronic nose has a housing retaining an array of metal-oxide semiconductor (MOS) gas sensors retained in the chamber of the housing. These sensors are capable of being saturated by a target gas to then produce a voltage drop across the sensors resulting in an output response in volts (V). The MOS-based sensors are capable of detecting gas

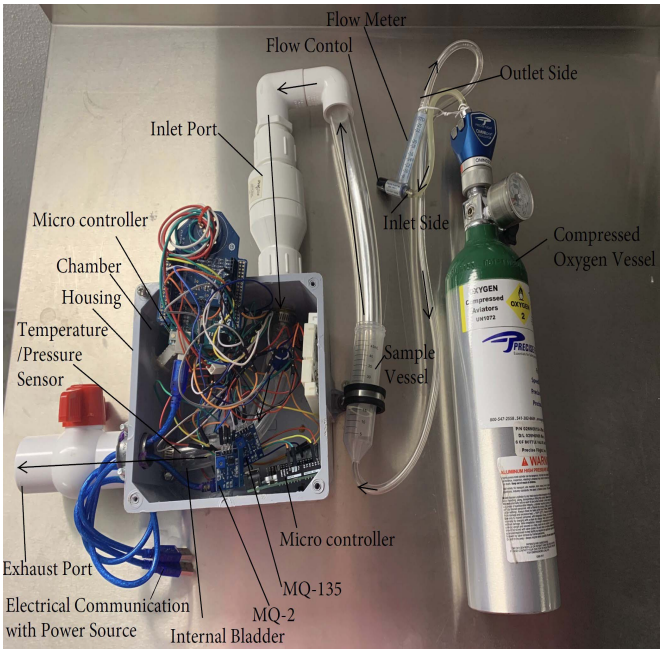

Fig. 1. Electronic nose having gas sensing components retained within an internal bladder being in communication with a sample vessel, compressed oxygen carrier gas, and a flowmeter.

concentrations in parts-per-million (ppm) of CO, acetone, and alcohol. Referring to Figure 1, circuitry of the first Arduino Uno microcontroller electrically connects to the MOS-based MQ-2 and MQ-135 gas sensors. The second Arduino Uno microcontroller is electrically connected to a BME280 sensor configured to measure pressure and temperature within the chamber of the housing. The housing chamber retains an internal bladder which connects the input port of the electronic nose to the exhaust port of the electronic nose to separate the microcontrollers and electronic circuitry from the gas obtained from the sample solution, whereby, at least a portion of the BME280, MQ-2 sensor configured to detect both CO and alcohol, and a MQ-135 sensor configured to detect acetone are retained within the internal bladder. The microcontrollers are electrically wired to a 5V power source being an electronic device such as a computer. The electronic device has a graphic user interface configured for a programmer to calibrate the gas sensors, to define threshold values, and to collect data pertaining to the detected gas signature.

B. Gas Detection Components

The internal bladder of the housing chamber is purged with compressed oxygen, as the carrier gas, to reset the sensors to baseline. A sample solution comprises liquid alcohol and liquid acetone mixed together and retained within an air tight sample vessel to reduce and/or eliminate environmental contaminants.

In an attempt to mimic the temperature of exhaled breath, the sample solution of liquid alcohol and liquid acetone were heated to approximately 94°F within the known range of 87.8°F-95°F for exhaled breath temperature [27]. Fig. 1 illustrates the orientation of the compressed oxygen vessel being in communication with the flow meter, the sample vessel retaining the simulated breath sample liquid solution, and the internal bladder of the electronic nose housing. The gasses emitted from the simulated breath sample liquid solution being retained within the sample vessel are carried by compressed oxygen to mix with 150 ppm of compressed CO calibration gas. The compressed CO gas is emitted from a controlled high pressure aluminum cylinder in communication with the sample vessel retaining the gasses emitted from the liquid alcohol and the liquid acetone solution. These gasses are then pumped into the internal bladder through a one-way valve of the inlet port. The t-handle of the ball valve of the exhaust port is oriented in a closed position to ensure the sample is retained in the internal bladder long enough to saturate the gas sensors.

The alcohol, CO, and acetone gasses mimic the mixture of gasses present in an exhaled breath and are carried with the compressed oxygen carrier gas past a single MOS-based MQ-2 sensor configured to detect both CO and alcohol, a single MOS-based MQ-135 sensor configured to detect acetone, and a BME280 sensor configured to detect temperature having a BMP280 piezo-resistive pressure sensor. The flow control of the model A-5 In-Line Dual Scale Flowmeter is configured for a user to visually monitor the volume of oxygen flow in milliliters per second (mL/s) via a round ball within the tapered tube of the flowmeter. The gas flows to the sensors which are mounted on an inner wall surface of the internal bladder near the inlet port of the electronic nose and the gas is then exhausted through the exhaust port of the electronic nose when the t-handle of the ball valve is oriented in an open position.

After the gasses emitted from the simulated breath sample solution saturate the sensors within the internal bladder of the electronic nose, the analog signal from the MQ-2 and MQ-135 sensors are transmitted to a LM393 High Precision Comparator configured to digitize the signal. The comparator determines when the threshold values set by the potentiometer of the sensors have been met. The sensors of the electronic nose interface with a microcontroller Arduino Uno and the sensor values of CO, alcohol, acetone concentrations are displayed on a serial monitor within approximately 27 seconds from the initial sample introduction. The Arduino Uno code converts the digital signal from output response (V) into concentration (ppm) based on the resistance ratio (R_S/R_0) of the resistance change when the sensor is exposed to a target gas (R_S) in relation to the stable sensor resistance of the sensor in clean air (R_0). Thus, a detected target gas of a sample may be detected and measured to indicate the approximate concentration in ppm.

III. Results and Discussion

A. Temperature, Pressure, and Flow Control

Fig. 2(a) shows the measured temperature detected from the BME280 temperature sensor and the baseline drift of the MQ-2 and MQ-135 sensors retained within the internal bladder of the electronic nose at the ambient working condition of temperature being approximately 66°F and having approximately 61% humidity after preheating for 24 hours. The baseline of the sensors output for both the MQ-2 and MQ-135 sensor

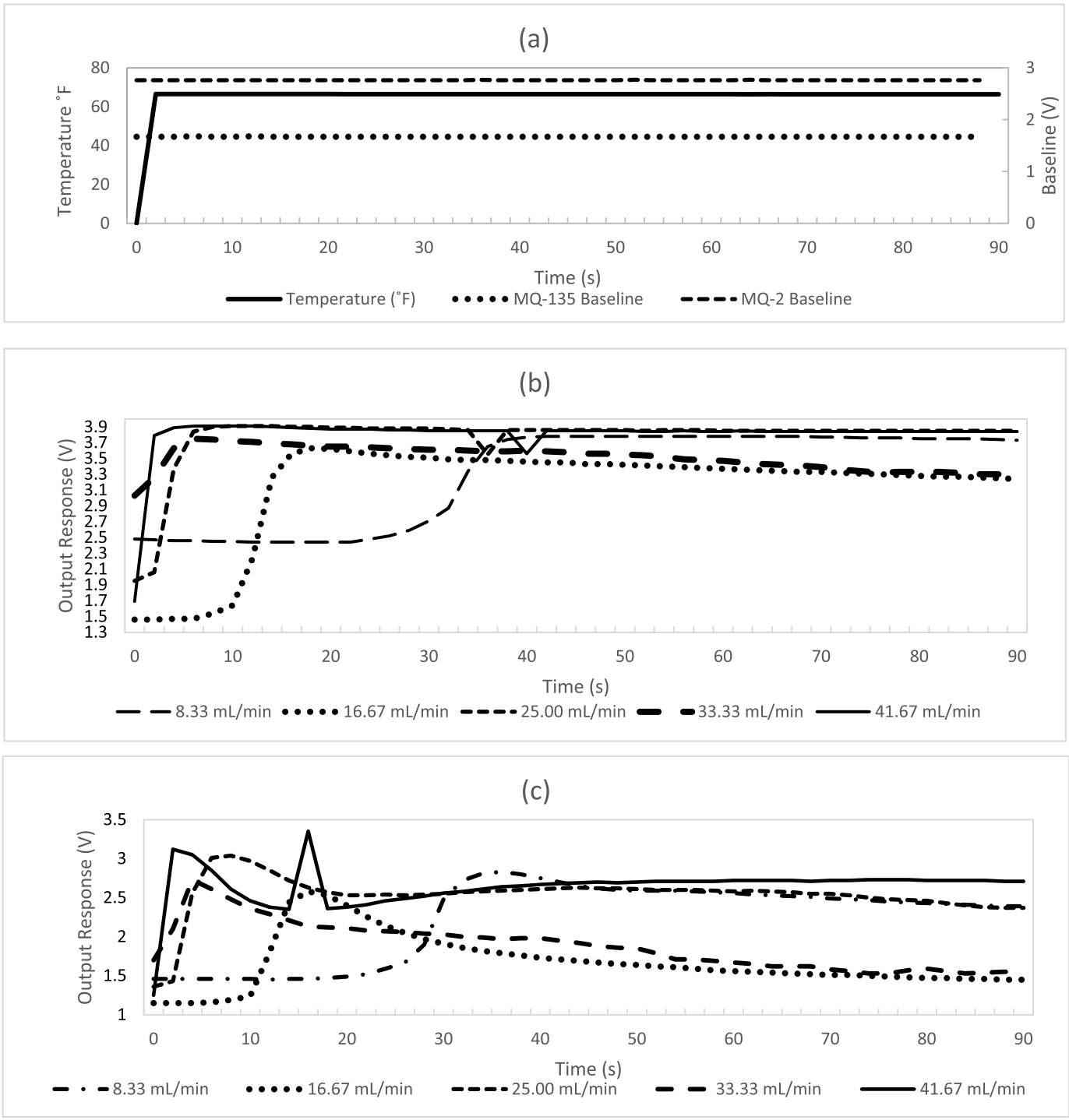

Fig. 2. (a) Temperature and flow control of baseline drift over the MQ-2 and MQ-135 MOS based sensors, (b) Output responses of the MQ-2 sensor at different flow rates of 300 ppm sample solution, (c) Output responses of the MQ-135 sensor at different flow rates of 300 ppm sample solution.

maintains a stable state at ambient working conditions for concentrations of CO, alcohol, and acetone. The flow rate of the carrier gas is regulated to dispense oxygen using the flow control of the flowmeter which may be rotated to adjust the flow of the carrier gas. Fig. 2(b) illustrates the resulting output responses of the MQ-2 sensor as the sensor is exposed to gasses emitted from 300 ppm of the sample solution at different flow rates. Fig. 2(c) illustrates the resulting output responses of the MQ-135 sensor as the sensor is exposed to gasses emitted from 300 ppm of the sample solution at different flow rates. For both the MQ-2 and MQ-125 sensors, as the flow rates increase, the characteristic peaks of alcohol, CO, and acetone, detected from the sample solution, occur more rapidly compared to when the flow rate is reduced. As the flow rate increases, the positions of the characteristic peaks of alcohol, CO, and acetone congregate in a closer proximity to each other compared to the peaks having a decreased flow rate. The peaks of the target gas have a closer proximity to each other during an increased flow rate result in an increased difficulty to differentiate between each target

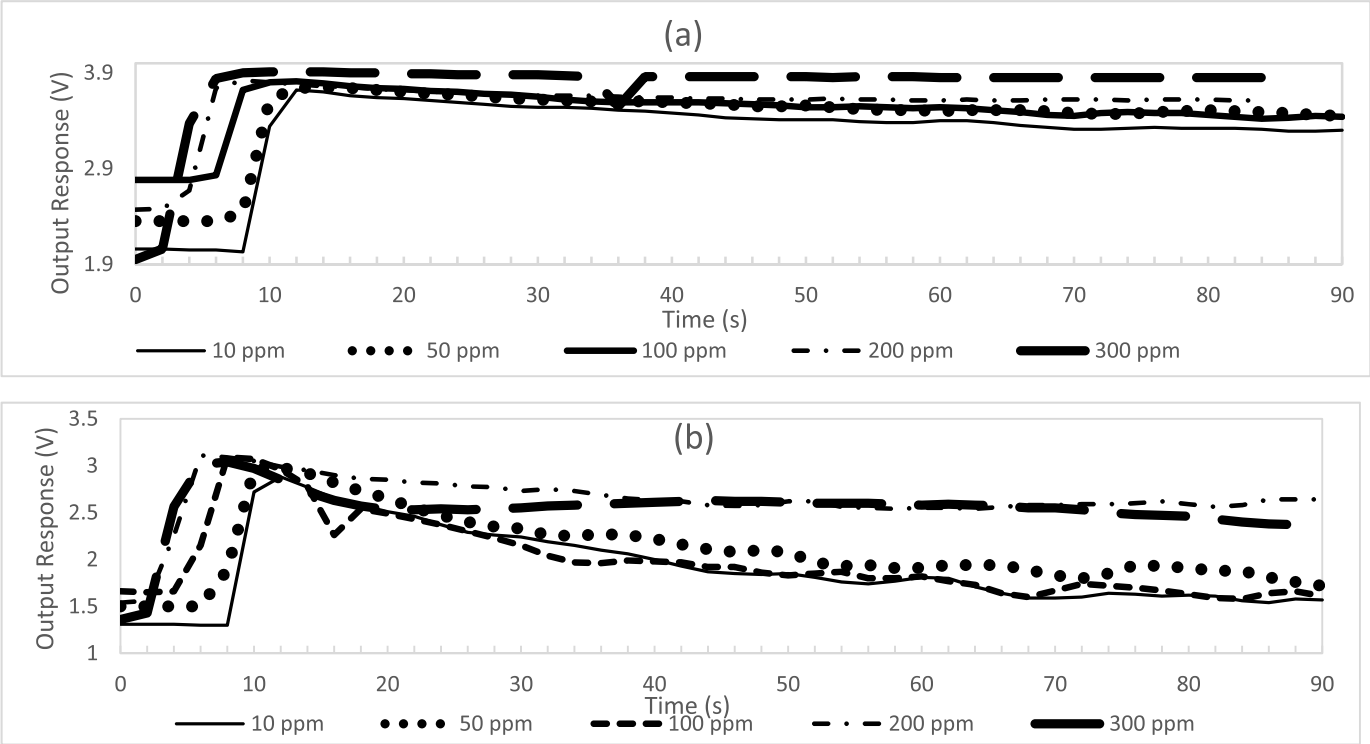

Fig. 3. Gas concentration gradient of simulated breath sample having a flow rate of 25.00 mL/min (a) for the MQ-2 sensor, (b) for the MQ-135 sensor.

gas during an increased flow rate. However, the detection of these peaks having a decreased flow rate require an increase in detection time for each detection protocol. Thus, it would be more desirable for an electronic nose to have a medium flow rate resulting in a more rapid detection of a target gas with minimal sample time for the sensors to return to baseline. Thus, in light of the measured output response and the detection time, the electronic nose proceeded with the more desirable protocol using the sample solution having a flow rate of the oxygen carrier gas being approximately 25.00 mL/s.

B. Gas Concentration Gradient

Fig. 3(a) illustrates the output response of the MQ-2 sensor having a concentration of the simulated breath sample solution with ranges between 10 ppm – 300 ppm having a flow rate of 25.00 mL/min. Fig. 3(b) illustrates the output response of the MQ-135 sensor having a concentration of the simulated breath sample solution with ranges between 10 ppm – 300 ppm having a flow rate of 25.00 mL/min. The detection range of concentrations of alcohol, acetone, and CO detected in the sample solution of the electronic nose was configured for a detection range of approximately 10 ppm-300 ppm according to the standard operating conditions of the sensors. As the flow rate increases, the detection time of both the MQ-2 and MQ-135 sensors decrease which is more desirable for rapid detection of target gasses. The output response of the MQ-2 sensor demonstrates an elevated output response as a result of an increased flow for all tested concentrations of sample solution between 10 ppm – 300 ppm. The output response of the MQ-135 sensor demonstrates an elevated output response as a result of an increased flow for tested concentrations of sample solution between 10 ppm – 200 ppm. The signal accuracy of

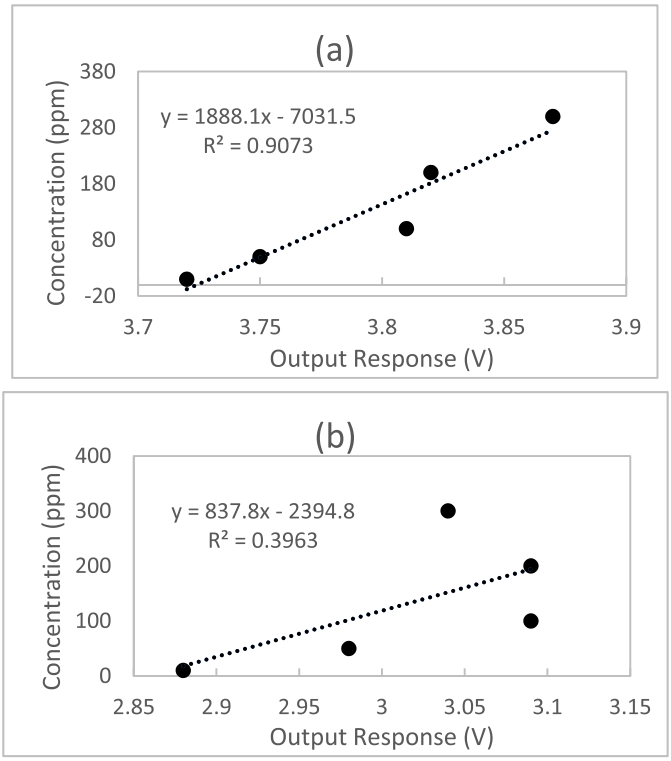

Fig. 4. Correlation analysis of the concentration gradient, (a) for the MQ-2 sensor, (b) for the MQ-135 sensor.

the of the MQ-135 sensor may be compromised from noise as the sample solution exceeds 200 ppm. The concentrations in ppm of alcohol, CO, and acetone are calculated after the output of the MQ-2 and MQ-135 sensors are converted by the code of the Arduino Uno microcontroller.

Regression analysis was performed to determine the linear model data between Time (s) and the Output Response (V) as illustrated in Fig. 4(a) for the MQ-2 sensor and in Fig. 4(b) for the MQ-135 sensor. The correlation between the values of the output response peaks and the concentration gradient of the sample solution have been determined and the fitting formula of Fig. 4(a) has measured relativity (R^2) showing the linear regression model fits the data set of the MQ-2 sensor with a $R^2 > 0.9073$. Thus, 90.73% of the variation in the output responses of the MQ-2 sensor results from the changes in concentration values of sample solution. Fig. 4(b) depicts the fitting formula having measured relativity (R2) indicating the linear regression model fits the data set of the MQ-135 sensor with a $R^2 > 0.3963$. 39.63% of the variation in the output responses of the MQ-135 sensor results from the concentration values of sample solution.

There is a substantial difference in the R^2 value of the MQ-2 sensor and the MQ-135 sensor indicating that the MQ-135 sensor may need to incorporate an improved low noise design to perform signal conditioning, digital signal processing, and pattern recognition to filter out the noise in an attempt to increase accuracy and efficiency of these sensors. In particular, the signal or detected inflammatory biomarker being detected by the MQ-135 sensor may be suppressed by background noise attributed to factors including, but not limited to, environmental factors, human factors, concentration value, or flow rate. Further, an air tight sample vessel and sensors retained within an air tight internal bladder within the chamber of the electronic nose housing may reduce the exposure of the sensors to noise that may contribute to crosstalk interference between gasses to improve accuracy of the output response voltage of the gas sensors.

C. Comparative Sensor Analysis

Unlike GC-IMS techniques currently used to separate the plurality of compounds in an exhaled breath sample and then identification of each individual compound based on drift velocity, MOS based MQ gas sensors of this instant study detect a target gas based on a voltage divider network formed by the load resistance and the sensor. The MQ-2 and MQ-135 sensors are coded using Arduino software configured to calculate specific gas concentrations using fresh air calibration data and the resistance ratio provided by the manufacturer's datasheet. In particular, the load resistance slope and intercept of the calibration line follow a linear scale that is converted into a log-log scale, as the MQ sensor data is nonlinear. The Arduino coding program utilized in this study calculates the resistance of the sensor from the analog voltage across the load resistor.

For example, the MQ-2 sensor has sensitivity characteristics for a plurality of gasses including, but not limited to, CO and alcohol, whereby, a single MQ-2 sensor produces an analog output voltage. Thus, a single MQ-2 sensor will not differentiate between a concentration of detected CO and a concentration of detected alcohol with a high accuracy. As a result, it is expected that the accuracy of the sensors will improve if a gas detection system has a first gas sensor having a high sensitivity to CO and a second gas sensor having a high sensitivity to alcohol rather than a single gas sensor having a broad detecting scope encompassing both CO and alcohol. Further, the incorporation of an array of sensors that are highly specific to an individual target gas is desirable for our future works in the evolution this current electronic nose system. However, in light of the sensitivity characteristics of the MQ sensors used in this instant study, the analysis of the unique characteristics of the output response of a single MQ-2 sensor to a diverse environment of target gasses, including CO and alcohol, is explored in this paper to determine the suitability of MQ sensors for the application of exhaled breath analysis in COVID-19.

Referring again to Figs. 2(b) and 3(a), the MQ-2 sensor output voltage data starting at 0 s has a baseline drift of approximately 2.8 V, whereby, electrons from the heated tin dioxide semiconductor particles of the sensing element interact with ambient air, ionize the oxygen in the air causing the tin dioxide to adsorb the oxygen and obstruct the electrical current flow through the sensing element of the MQ-2 sensor. At 6 s of exposure to the simulated exhaled breath sample gas, an increase in the measured output voltage occurs at 3.7 V from the MQ-2 sensor. In particular, this voltage increase occurs when the adsorbed oxygen becomes saturated by the CO and alcohol gas mixture and is cleaved from its communication with the tin dioxide semiconductor particles of the sensor, whereby, facilitating unobstructed current flow through the sensing element and an associated resistance change of an increased output voltage. As shown in Fig. 5, during this voltage increase, the MQ-135 sensor detected peaks of approximately 18 ppm acetone and the MQ-2 sensor detected peaks of 42 ppm CO and 15 ppm alcohol from the 300 ppm sample solution at a flow rate of 25.00 mL/min for 30 s.

Most apparent after 10 s, the output response voltage of the MQ-2 sensor has a gradual decline as the CO and alcohol gas mixture begin to dissipate to a lower concentration level. This gradual decline in output response voltage is facilitated as newly available electrons from the heated tin dioxide semiconductor particles of the sensor ionize the oxygen in the air. The sensor adsorbs the ionized oxygen and obstructs the electrical current flow through the sensing element of the MQ-2 sensor until the baseline drift of approximately 2.8 V is achieved. In Figs. 2(b) and 3(a), the output response of the MQ-2 sensor has not declined to meet its baseline drift of approximately 2.8 V even at 90 s. In contrast, the MQ-135 sensor reaches its approximate baseline drift of 1.8 V, at a faster rate, of approximately 50 s as illustrated in Figs. 2(c) and 3(b). This time dependent characteristic is indicative that an MQ-2 sensor with a wide scope of detection for a plurality of gasses within a sample of diverse gasses will take a longer length of time to reach baseline drift compared to an MQ-135 sensor with a higher selectivity for a single gas within a sample of diverse gasses. This process may be expedited by purging the system with compressed oxygen to remove the gasses more quickly from the internal bladder of the electronic nose between sampling intervals.

The design of the electronic nose platform has been constructed to minimize the impact of crosstalk interference of gasses upon the gas sensors. In particular, as a result of the

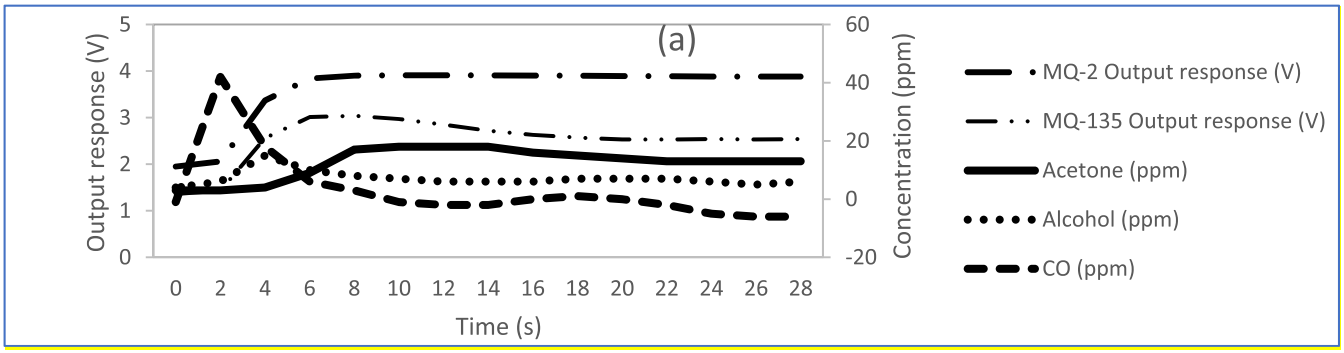

Fig. 5. Output response voltages from of the MQ-2 sensor and the MQ-135 sensor with associated individual gas concentrations in ppm of acetone, alcohol, and CO from the 300 ppm sample solution at a flow rate of 25.00 mL/min for 30 s.

interactions of differing gasses within the simulated sample of exhaled breath and the crosstalk interference that occurs with these gasses at the sensing element of the MQ-2 sensor compared to the MQ-135 sensor, the accuracy of an electronic nose system for the application of exhaled breath analysis would be enhanced by having an array of gas sensors each having a high sensitivity and high selectivity to a single target gas rather than having a wide detection scope of gases.

D. Detection Method

It would be desirable for a gas analysis system to indicate to a user when concentrations within an exhaled breath fall within a suitable range considered to be a breath pattern signature of COVID-19, whereby, elevated concentrations of CO and acetone combined with the lowered concentration of alcohol are detected in COVID-19 breath samples and are not characteristic of non-COVID-19 breath samples. In order to accomplish incorporating a light emitting unit indicator to the current electronic nose system to accurately activate in response to both the CO and alcohol concentrations detected within a sample, a first gas sensor having a high sensitivity to CO and a second gas sensor having a high sensitivity to alcohol would need to be provided. For example, CO emitted from a non-COVID-19 breath sample has a concentration range of approximately 2 ppm – 100 ppm, corresponding to a "healthy" signature [14]. When a first gas sensor, having a high sensitivity to CO, detects a concentration value of CO emitted from the simulated breath sample solution having a value over 100 ppm, the red colored light emitting diode (LED) of the breath chamber housing of the electronic nose will illuminate to indicate a potential inflammatory response symptom of COVID-19.

In another example, Table I shows alcohol emitted from the a non-COVID-19 breath sample has a concentration range between 0.4 ppm – 2.0 ppm, corresponding to a "healthy" signature [15]. When a second gas sensor, having a high sensitivity to alcohol, detects a concentration value of alcohol emitted from the simulated breath sample solution having a value less than 0.4 ppm, the green LED of the breath chamber housing of the electronic nose will illuminate to indicate a potential inflammatory response symptom of COVID-19. Since the sensitivity characteristics of the MQ-2 sensor have a broad detection range for alcohol, this sensor was calibrated to increase sensitivity by rotating the potentiometer clockwise.

In yet another example, the MQ-135 sensor of Table I is configured to detect a concentration of acetone. Acetone emitted from a non-COVID-19 breath sample has a concentration range between 0.24 ppm – 1.69 ppm, corresponding to a "healthy" signature. When the MQ-135 sensor detects a concentration value of acetone emitted from the simulated breath sample solution having a value over 2.0 ppm, the yellow LED will illuminate to indicate a potential inflammatory response symptom of COVID-19. In a preferred embodiment, if the target gas concentrations in the sample of exhaled breath exceeds threshold values of at least 2 gas sensors, this may be a strong indication of presence of an inflammatory response associated with COVID-19.

IV. Conclusion and Future Work

The sampling and analysis of exhaled breath to determine a variety of biomarkers in disease has been explored. These investigations are implemented to gain a noninvasive insight to the diagnosis and the monitoring of progression of diseases such as lung disease, airway inflammatory disease, liver disease, and viral induced diseases such as COVID-19. Structural configuration and sensor array materials of the electronic nose devices have been shown to impact the gas sensor accuracy and selectivity for a target gas as it relates to a desired signature of disease in simulated COVID-19 breath sample analysis. Further, the sensor type, the concentration of sample solution, and flow of the electronic nose system have been shown to influence the amount of CO, alcohol, and acetone gas detected. The measured quantity of a plurality of detected gasses within breath ultimately defines a unique signature over time.

To date, the direct link between SARS-CoV-2 gaining access to the nervous system through the olfactory nerve to invoke reversible anosmia and COVID-19 induced pediatric inflammatory multisystem syndrome remains unexplored and represents a major gap in knowledge about SARS-CoV-2 cellular entry and associated detectable biomarkers of COVID-19. Thus, we propose to elucidate the olfactory nerve's role in viral entry of SARS-CoV-2 to the nervous system and determine further quantitative biomarkers associated its immune response in an effort to gain insights in expanding the scope of the breath pattern signature of detecting COVID-19. We posit that a highly specified sensor array detection system may be capable of identifying inflammatory biomarkers of COVID-19 from the breath of an individual. Accordingly, we will probe the role

of electrochemical and semiconductor-based detection sensors as well as canine detection of these viral components and/or inflammatory biomarkers under ambient and pathological conditions. Although there are ongoing efforts in breath analysis research addressing the standardization sampling, analytic, and reporting to correlate the data of the studies so that the data may be better interpreted, modifications to existing electronic nose devices are required to address the signal suppression problem as for example, the MQ-135 sensor may have demonstrated.

ACKNOWLEDGMENT

The authors thank the University of South Florida COVID-19 Rapid Response Research Grants program and the efforts made by the University of South Florida researchers and breath specialists based in Edinburgh, U.K., in Dortmund, Germany, and in Jacksonville, FL, USA, for their contributions to high impact research and public service during this global pandemic.

REFERENCES

[1] A. Wilson, "Advances in electronic-nose technologies for the detection of volatile biomarker metabolites in the human breath," *Metabolites*, vol. 5, no. 1, pp. 140–163, Mar. 2015, doi: 10.3390/metabo5010140.

[2] S. G. Waxman, "Axonal conduction and injury in multiple sclerosis: The role of sodium channels," *Nature Rev. Neurosci.*, vol. 7, no. 12, pp. 932–941, 2006.

[3] M. K. Galougahi, J. Ghorbani, M. Bakhshayeshkaram, A. S. Naeini, and S. Haseli, "Olfactory bulb magnetic resonance imaging in SARS-CoV-2-induced anosmia: The first report," *Academic Radiol.*, vol. 27, no. 6, pp. 892–893, Jun. 2020, doi: 10.1016/j.acra.2020.04.002.

[4] H. Chen *et al.*, "Breath-borne VOC biomarkers for COVID-19," *Res. Gate*, to be published, doi: 10.1101/2020.06.21.20136523.

[5] L. Cipollaro, L. Giordano, J. Padulo, F. Oliva, and N. Maffulli, "Musculoskeletal symptoms in SARS-CoV-2 (COVID-19) patients," *J. Orthopaedic Surg. Res.*, vol. 15, no. 1, pp. 1–7, May 2020, doi: 10.1186/s13018-020-01702-w.

[6] S. Boesveldt *et al.*, "Anosmia—A clinical review," *Chem. Senses*, vol. 42, no. 7, pp. 513–523, 2017, doi: 10.1093/chemse/bjx025.

[7] A. Marinosci, B. N. Landis, and A. Calmy, "Possible link between anosmia and COVID-19: Sniffing out the truth," *Eur. Arch. Oto-Rhino-Laryngol.*, vol. 277, pp. 2149–2150, Apr. 2020, doi: 10.1007/s00405-020-05966-0.

[8] D. van Riel, R. Verdijk, and T. Kuiken, "The olfactory nerve: A shortcut for influenza and other viral diseases into the central nervous system," *J. Pathol.*, vol. 235, no. 2, pp. 277–287, Jan. 2015, doi: 10.1002/path.4461.

[9] B. Henderson *et al.*, "A benchmarking protocol for breath analysis: The peppermint experiment," *J. Breath Res.*, vol. 14, no. 2, 2020, Art. no. 046008, doi: 10.1088/1752-7163/aba130.

[10] S. D. Roper, "Gustatory and olfactory sensory transduction," in *Cell Physiology Source Book*, N. Sperelakis, Ed., 4th ed. New York, NY, USA: Academic, 2012, pp. 681–697. [Online]. Available: http://www.sciencedirect.com/science/article/pii/B9780123877383000391, doi: 10.1016/B978-0-12-387738-3.00039-1.

[11] L. Wang *et al.*, "Clinical manifestations and evidence of neurological involvement in 2019 novel coronavirus SARS-CoV-2: A systematic review and meta-analysis," *J. Neurol.*, vol. 267, pp. 2777–2789, Jun. 2020, doi: 10.1007/s00415-020-09974-2.

[12] M. Palao, E. Fernández-Díaz, J. Gracia-Gil, C. M. Romero-Sánchez, I. Díaz-Maroto, and T. Segura, "Multiple sclerosis following SARS-CoV-2 infection," *Multiple Sclerosis Rel. Disorders*, vol. 45, Oct. 2020, Art. no. 102377, doi: 10.1016/j.msard.2020.102377.

[13] W. Miekisch, J. K. Schubert, and G. F. E. Noeldge-Schomburg, "Diagnostic potential of breath analysis—Focus on volatile organic compounds," *Clinica Chim. Acta*, vol. 347, nos. 1–2, pp. 25–39, 2004. [Online]. Available: https://ebscohost.com/login.aspx?direct=true&db=edsbl&AN=RN153916388&site=eds-live

[14] B. D. Cox and M. J. Whichelow, "Carbon monoxide levels in the breath of smokers and nonsmokers: Effect of domestic heating systems," *J. Epidemiol. Community Health*, vol. 39, no. 1, pp. 75–78, Mar. 1985. [Online]. Available: http://search.ebscohost.com.ezproxy.lib.usf.edu/login.aspx?direct=true&db=edsjsr&AN=edsjsr.25566538&site=eds-live

[15] J. D. Fenske and S. E. Paulson, "Human breath emissions of VOCs," *J. Air Waste Manage. Assoc.*, vol. 49, no. 5, pp. 594–598, 1999. [Online]. Available: http://search.ebscohost.com.ezproxy.lib.usf.edu/login.aspx?direct=true&db=edsbl&AN=RN061130263&site=eds-live

[16] J. C. Anderson, "Measuring breath acetone for monitoring fat loss: Review," *Obesity*, vol. 23, no. 12, pp. 2327–2334, 2015. [Online]. Available: http://search.ebscohost.com.ezproxy.lib.usf.edu/login.aspx?direct=true&db=edsbl&AN=RN374828987&site=eds-live

[17] D. M. Ruszkiewicz *et al.*, "Diagnosis of COVID-19 by analysis of breath with gas chromatography-Ion mobility spectrometry—A feasibility study," *EClinicalMedicine*, vols. 29–30, Dec. 2020, doi: 10.1016/j.eclinm.2020.100609.

[18] M. E. Hartman *et al.*, "COVID-19 respiratory failure: Targeting inflammation on VV-ECMO support," *ASAIO J.*, vol. 66, no. 6, pp. 603–606, Jun. 2020, doi: 10.1097/MAT.0000000000001177.

[19] C. Y. Cheung *et al.*, "Cytokine responses in severe acute respiratory syndrome coronavirus-infected macrophages *in vitro*: Possible relevance to pathogenesis," *J. Virol.*, vol. 79, no. 12, pp. 7819–7826, 2005.

[20] M. Vaduganathan *et al.*, "Renin–angiotensin–aldosterone system inhibitors in patients with COVID-19," *New England J. Med.*, vol. 382, no. 17, pp. 1653–1659, Apr. 2020. [Online]. Available: https://www.nejm.org/doi/full/10.1056/NEJMsr2005760J, doi: 10.1056/NEJMsr2005760.

[21] E. J. Molloy and C. F. Bearer, "COVID-19 in children and altered inflammatory responses," *Pediatric Res.*, vol. 88, no. 3, pp. 340–341, Sep. 2020, doi: 10.1038/s41390-020-0881-y.

[22] R. W. Paterson *et al.*, "The emerging spectrum of COVID-19 neurology: Clinical, radiological and laboratory findings," *Brain*, vol. 143, no. 10, pp. 3104–3120, Oct. 2020, doi: 10.1093/brain/awaa240.

[23] S. Kremer *et al.*, "Brain MRI findings in severe COVID-19: A retrospective observational study," *Radiology*, vol. 297, no. 2, pp. E242–E251, Nov. 2020, doi: 10.1148/radiol.2020202222.

[24] F. J. H. Ramos, A. P. García, and M. D. J. Hernández, "Neurology during the pandemic. Is COVID-19 changing the organisation of neurology departments?" *Neurología (English Ed.)*, vol. 35, no. 4, pp. 269–271, May 2020. [Online]. Available: https://doi-org.ezproxy.lib.usf.edu/10.1016/j.nrleng.2020.04.008

[25] G. Toscano *et al.*, "Guillain–Barré syndrome associated with SARS-CoV-2," *New England J. Med.*, vol. 382, no. 26, pp. 2574–2576, Jun. 2020, doi: 10.1056/NEJMc2009191.

[26] T. Moriguchi *et al.*, "A first case of meningitis/encephalitis associated with SARS-coronavirus-2," *Int. J. Infectious Diseases*, vol. 94, pp. 55–58, May 2020, doi: 10.1016/j.ijid.2020.03.062.

[27] E. Mansour *et al.*, "Measurement of temperature and relative humidity in exhaled breath," *Sens. Actuators B, Chem.*, vol. 304, Feb. 2020, Art. no. 127371.

Tiffany C. Miller received the Bachelor of Science degree in bio-medical sciences and the Master of Science degree in engineering science. She is currently pursuing the Ph.D. degree in electrical engineering with the University of South Florida (USF). Her qualifications have been mastered by achieving the passing of the examination for registration to practice in patent cases before the United States Patent and Trademark Office and known informally as the Patent Bar. Her USPTO Registration No. 63,465 brings her skills and expertise to Inventions International Inc., where she has been a Top Patent Practitioner and a Proud Member of the Patent Bar, since 2008. She is permitted to prepare an application for a patent and conduct the prosecution before the United States Patent and Trademark Office.

Salvatore Domenic Morgera (Life Fellow, IEEE) received the bachelor's, master's, and Ph.D. degrees from Brown University, Providence, RI, USA. He has focused on networks in his entire professional life. He and his teams are responsible for the Canadian oceanographic data gathering networks, the acoustic networks for American submarine tactical and strategic communications, the worldwide CAT3 auto-landing networks for commercial aircraft, the military wireless networks used in sensitive and challenging parts of the world, and the intelligent AI-enhanced pathogen wireless sensor networks used in public health facilities. In the last decade, he has turned his attention to the neurological networks of the brain and its electric near-field and bio-metamaterial structures. He has challenged his multidisciplinary team with understanding these extraordinary near-field networks and the bio-metamaterial human brain structure in which they operate. He is a Professor of Electrical Engineering with the University of South Florida, a Tau Beta Pi Eminent Engineer, an Emeritus Professor at Universities in Canada and USA, and the Director of the Global Center for Neurological Networks. Dr. Morgera has published 290 fully refereed articles in journals and conference proceedings and three books, two of which are research monographs, and 72 Government research reports and white papers. He has over 26 patents. He is a Fellow of the American Association for the Advancement of Science (AAAS), and the Institution for Engineering and Technology (IET) for his many years in University administration, development of a graduate bioengineering degree program, which has become a model for the nation, and advances in our understanding of brain structure and function. Recently, he has been invited to give two keynote speeches at international conferences on the topic of brain structure and function.

Stephen E. Saddow (Senior Member, IEEE) received the Ph.D. degree in electrical engineering from the University of Maryland at College Park in 1993. He is currently a Professor with the Department of Electrical Engineering and the Department of Medical Engineering at the University of South Florida (USF), Tampa, FL, USA. He is also a Collaborating Scientist at the Italian Synchrotron Light Source (Elettra, Beamline BEAR), and a Guest Researcher at the National Cancer Institute. He was elected as a Fellow of the AIMBE for seminal contributions to the field of silicon carbide (SiC) biomedical technology, significantly advancing in vivo biomedical devices and systems. Dr. Saddow is a Senior Member of the National Academy of Inventors and holds more than 15 patents, mostly on SiC biomedical device technology.

Arash Takshi graduated in electronics from the Amirkabir University of Technology, Iran, in 1993. He received the M.Sc. degree in analog electronics from the Sharif University of Technology, Tehran, in 1996, and the Ph.D. degree in organic electronics from The University of British Columbia (UBC), Canada, in 2007. From 2007 to 2009, he was a Postdoctoral Fellow with the UBC, working on biophotovoltaic devices. He is currently an Associate Professor of Electrical Engineering with the University of South Florida (USF).

Matthew Palm received the bachelor's degree in technical management. He is a Managing Partner and COO with Valhall k- 9 International. He is responsible for operations management and government contracting. He is the U.S. Navy Veteran, who spent most of his career with a military flight simulation manufacturing and training company. In his career, he has performed duties relating to solution architecture, capture/proposal management, program management, process analysis, change management, technical writing, and training instructor.